
**Liquid Crystals**
Publication details, including instructions for authors and subscription information:
http://www.informaworld.com/smpp/title~content=t713926090

# Microdielectrometric monitoring of film preparation process with oriented domains for hydroxypropyl cellulose cast from isotropic aqueous solution under the sinusoidal electric field with large amplitude

Katsufumi Tanaka[a]; Yuichiro Tanabe[a]; Ryuichi Akiyama[a]
[a] Department of Macromolecular Science and Engineering, Graduate School of Science and Technology, Kyoto Institute of Technology, Matsugasaki, Kyoto 606-8585, Japan

**To cite this Article** Tanaka, Katsufumi , Tanabe, Yuichiro and Akiyama, Ryuichi(2008) 'Microdielectrometric monitoring of film preparation process with oriented domains for hydroxypropyl cellulose cast from isotropic aqueous solution under the sinusoidal electric field with large amplitude', Liquid Crystals, 35: 8, 937 — 951
**To link to this Article: DOI:** 10.1080/02678290802304919
**URL:** http://dx.doi.org/10.1080/02678290802304919

*Liquid Crystals,*
Vol. 35, No. 8, August 2008, 937–951

Taylor & Francis
Taylor & Francis Group

# Microdielectrometric monitoring of film preparation process with oriented domains for hydroxypropyl cellulose cast from isotropic aqueous solution under the sinusoidal electric field with large amplitude

Katsufumi Tanaka*, Yuichiro Tanabe and Ryuichi Akiyama

*Department of Macromolecular Science and Engineering, Graduate School of Science and Technology, Kyoto Institute of Technology, Matsugasaki, Kyoto 606-8585, Japan*

*(Received 20 October 2007; final form 25 June 2008)*

Microdielectrometry was applied to macroscopically anisotropic media. The distribution and effective portion of the electrostatic energy density, $w_{14}$ and $J_{14}$, respectively, were calculated, considering the additive contributions of four pairs of microelectrodes. The electric field lines were calculated numerically and investigated experimentally with polarised optical microscopy using thin layers of a nematic liquid crystal with a positive dielectric anisotropy. The applicability of microdielectrometry was investigated using the nematic liquid crystal. Microdielectrometric monitoring was also performed during the preparation process for a solid film with oriented domains with long axes perpendicular to the electric filed cast from an isotropic aqueous solution of hydroxypropyl cellulose under the sinusoidal electric field with large amplitude of $2.0\,\mathrm{kV\,mm^{-1}}$ and frequency of $10^5$ Hz. In the logarithmic relation between the dielectric constant and loss factor divided by $J_{14}$, the two dielectric parameters measured for different film thicknesses at $2.0\,\mathrm{kV\,mm^{-1}}$ were superposed on a single curve. The curve for the electrically oriented domains was considrably different from that for a randomly oriented polydomain texture found under the electric field with small amplitude of $0.05\,\mathrm{kV\,mm^{-1}}$ and the same frequency.

**Keywords:** microdielectrometry; hydroxypropyl cellulose; cast films; electrical orientation



## 1. Introduction

Hydroxypropyl cellulose (HPC) is known as a lyotropic liquid crystal with a cholesteric phase structure in concentrated solutions (*1–6*). In aqueous solutions, the HPC molecules act like partially flexible rods because of intramolecular hydrogen bonding (*7*). The dielectric relaxation of the aqueous solutions at lower frequencies is affected by electrode polarisation and ionic conduction, and important relaxations including a rotational diffusion about the minor axis (the longitudinal rotation) of a partially flexible rod are usually screened out. On the other hand, a rotational diffusion of the rod with side chains about the major axis (the transversal rotation) was detected at higher frequencies. A local motion of chain segments in the relatively flexible rod was also detected as a longitudinal component and/or a transversal component confined even in the concentrated solutions (*5*).

An aqueous solution of 70 wt% HPC showed broad relaxations around $10^6$ Hz and at frequencies lower than $10^4$ Hz (*5*). The broad relaxation at the lower frequencies was partially related to the limited angular diffusion of a rod (the longitudinal rotation) within a virtual cone (*8*). The relaxation around $10^6$ Hz was related to the transversal rotational diffusion of a partially flexible rod with side chains, as well as a local motion of chain segments confined in the concentrated solution (*9, 10*). In addition, a negative dielectric anisotropy of $\Delta\varepsilon$ $(=\varepsilon_{//}-\varepsilon_{\perp})<0$ is expected, at least locally, at frequencies around $10^5$ Hz for the HPC solution, where $\varepsilon_{//}$ and $\varepsilon_{\perp}$ are the principal permittivities (or relative dielectric constants) parallel and perpendicular to the director, respectively. The longitudinal rotation is sufficiently relaxed in the concentrated solution, whereas the transversal rotation is still active around the frequencies. Similar relaxations have been reported even for solid films of HPC (*11, 12*).

In view of materials engineering, HPC is concentrated as the water solvent is removed during the preparation process of a solid film cast from an isotropic aqueous solution, so that the solid film would be prepared on a substrate from the isotropic solution via its liquid crystalline phase. Generally, the anisotropic solutions of liquid crystalline polymers show randomly oriented polydomain textures in the quiescent state (*4*) and shear-induced textures or banded texture after shearing (*5, 13, 14*). Because these macroscopic textures are closely related to the macroscopic physical properties, preparation methods for the monodomain texture and for a solid film that keeps such a texture are highly desired. The application of electric field during the preparation process is a possible method to obtain such a texture.

*Corresponding author. Email: ktanaka@kit.ac.jp

ISSN 0267-8292 print/ISSN 1366-5855 online

DOI: 10.1080/02678290802304919
http://www.informaworld.com

Up to now, a dc electric field (or a sinusoidal electric field with low frequency) was applied in most cases to solutions composed of rod-like molecules in organic solvents (*15–18*). The dielectric anisotropy of these solutions is considered to be positive at frequencies, including the static limit, corresponding to the applied electric fields, and the long axes of rod-like molecules were oriented along the electric field. In addition, some solid films thus prepared showed second harmonic generation in their nonlinear optical responses (*16, 18*), with lack of a centre symmetry for a polar structure. On the other hand, it is expected that the orientation of the long axes perpendicular to the electric field reported for liquid crystals of small molecules (*19, 20*) is induced by the electric field for the cast film of a liquid crystalline polymer with a negative dielectric anisotropy.

For aqueous solutions, it is widely known that the dc electric field (or the sinusoidal electric field of low frequency) cannot be applied sufficiently because of the conduction current. Little attention has been paid to the macroscopic orientation of anisotropic domains by the electric field cast from aqueous solutions. However, the aqueous solutions of HPC have become increasingly important since both the polymer and water solvent are environmentally friendly. Electrically induced orientation of anisotropic domains of HPC cast from the aqueous solutions is of current interest, both scientifically and environmentally. It is expected that the large amplitude of sinusoidal electric field of high frequency can be successfully applied to aqueous solutions of HPC. At such frequency, the conduction current is sufficiently suppressed and the dielectric anisotropy can be negative. It is additionally expected that the longitudinal rotation will be relaxed, whereas the transversal rotation of a partially flexible rod is still active for the HPC molecules (*5*). The transversal rotation of an HPC molecule is then induced by the electric field and an angular momentum about the long axis is also induced, giving a steady state for the long axis perpendicular to the electric field. At the same time, the in-situ monitoring of the preparation process of solid films is also desired for precise control of the textures (*21–26*).

In a previous paper (*27*), microdielectrometry (*22–26*) was used for the in-situ monitoring of the preparation process of a solid film with a randomly oriented polydomain texture cast from an isotropic aqueous solution of 30 wt % HPC under the sinusoidal electric field of small amplitude and frequency of $10^5$ Hz. The apparent dielectric constant, $\varepsilon_r'$, and loss factor, $\varepsilon_r''$, monotonically decreased with time as the water solvent was removed, because the dielectric constant of the water solvent is much larger than that of HPC at that frequency (*5*). During the process, the thickness of the wet film is gradually decreased as the solvent is removed. Therefore, the distribution and effective portion of the electrostatic energy density above the sensor surface, $w$ and $J$, respectively, were estimated, assuming a pair of semi-infinite planes halfway between the electrodes. Interestingly, the logarithmic relation between the two parameters measured for different film thicknesses were superposed on a single curve when they were divided for normalisation by an effective portion of the electrostatic energy density $J(d_D/D)$, where $d_D$ is each solid-film thickness and $D$ is the gap distance between the electrodes. It is suggested that the sample within a characteristic (or penetration) depth of the electrostatic energy density $(d/D)_{1/2}$ to give $J=1/2$ is mainly affected by the electric field. It is expected that macroscopic orientation of anisotropic domains with the long axes perpendicular to the electric field (*19, 20*) is induced in a film of HPC with a thickness on the order of $(d/D)_{1/2}$ by the electric field with large amplitude and frequency of $10^5$ Hz.

For the microdielectrometric monitoring of macroscopically anisotropic media, Fodor and Hill (*26*) showed the measured dielectric permittivity, $<\varepsilon>$, for a heterogeneous, anisotropic dielectric placed in a non-uniform electric field as the energy-density average of the permittivity over the volume pervaded by the field. For a uniaxial liquid crystal with a constant order parameter, $<\varepsilon>$ can be written as follows:

$$\begin{aligned}\langle\varepsilon\rangle &= \varepsilon_\perp + (\varepsilon_{//} - \varepsilon_\perp)\int_V \Phi(\mathbf{r})\cos^2\theta d\mathbf{r}^3 \\ &= \varepsilon_\perp + (\varepsilon_{//} - \varepsilon_\perp)\langle\cos^2\theta\rangle,\end{aligned} \tag{1}$$

$$\Phi(\mathbf{r}) = \frac{[\mathbf{E}(\mathbf{r})]^2}{\int_V [\mathbf{E}(\mathbf{r})]^2 d\mathbf{r}^3}, \tag{2}$$

where $\mathbf{E}(\mathbf{r})$ is the electric field at a position $\mathbf{r}$, $\Phi(\mathbf{r})$ is an energy density distribution function over the volume V pervaded by the field, and $\theta=\theta(\mathbf{r})$ is the local angle between the electric field and the director. Equation (1) defines the averaged orientation parameter $<\cos^2\theta>$. Locally, the director of the sample with a positive dielectric anisotropy tends to orient parallel to the electric field line, whereas that with a negative dielectric anisotropy tends to orient perpendicular to the electric field line.

In the present study, microdielectrometry has been applied to macroscopically anisotropic media. In the first place, the distribution and effective portion of the electrostatic energy density, $w_{14}$ and

$J_{14}$, respectively, are calculated by taking into account the additive contributions of four pairs of microelectrodes, as described in Appendix A. The electric field lines are also calculated numerically (*28*), as shown in Appendix B. Experimentally, the behaviour of the electric field lines has been investigated with polarised optical microscopy (POM) using thin layers of a nematic liquid crystal, 4,4′-*n*-pentylcyanobiphenyl (5CB) with a positive dielectric anisotropy (*29, 30*). Applicability of the microdielectrometry to macroscopically anisotropic samples of 5CB has also been investigated. Secondly, the microdielectrometric monitoring is reported for the preparation process of a solid film with oriented domains cast from an isotropic aqueous solution of HPC under the electric field with large amplitude and frequency of $10^5$ Hz. It is of great interest that anisotropic domains have been oriented with the long axes of the rod-like molecules perpendicular to the electric field. A logarithmic relation between the measured dielectric constant and the loss factor divided for normalisation by the effective portion of the electrostatic energy density $J_{14}$ is also reported, the similarities and differences of which are discussed in comparison with that for a randomly oriented polydomain texture found under the electric field with small amplitude and the same frequency.

## 2. Experimental

HPC was purchased from Sigma-Aldrich, Inc. The weight-averaged molecular weight, $M_w$, was approximately 80 000 and the number-averaged molecular weight, $M_n$, was approximately 10 000, with moles of substitution (MS) of 3.5. Distilled water was used to prepare the isotropic solutions with a polymer concentration of 30 wt% (*5, 27*). The wet films of the solutions were applied at room temperature onto the microdielectric sensor (*27*) using applicators for the thicknesses of the wet film ($d_W$) from 100 µm to 500 µm. The thickness of the solid films ($d_D$) was also measured using a dial gauge. The room temperature and relative humidity were monitored using a digital thermo-hygrometer. In addition, the applicability of the microdielectrometry was investigated experimentally using 4,4′-*n*-pentylcyanobiphenyl (5CB) (Merck, K-15) as a model liquid crystal of small molecules with a well-known positive dielectric anisotropy (*29, 30*).

In the present study, glass substrates with transparent interdigitated electrodes of tin-doped indium oxide (ITO) were used as the microdielectric sensor (*27*). Four pairs of ITO electrodes were sputtered on a glass slide with a gap distance ($D$) between the electrodes of 50 µm. The width ($W$) of the electrodes was 1.2 mm. The face-to-face length ($L$) for a pair of high voltage ($V^*$) and ground ($G$) electrodes was 10.5 mm, and the paired electrodes are numbered as shown in Figure A1a.

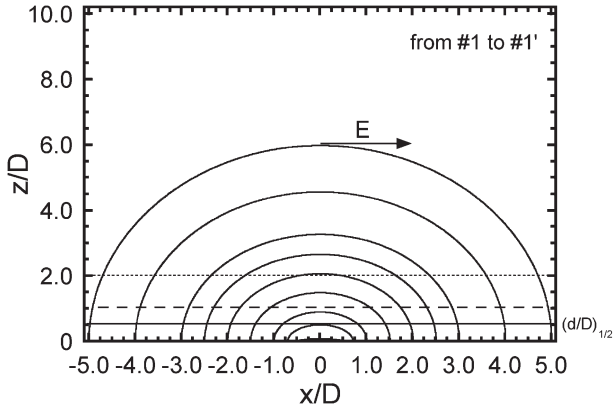


Figure 1. The electric field lines above the microdielectric sensor at a time corresponding to that shown in Figure A1b, the calculations for which are briefly discussed in Appendices A and B. Typical film thicknesses in the present study are indicated by the solid, broken and dotted lines.

The sinusoidal electric field with preset amplitude and frequency of 2.0 V µm$^{-1}$ (kV mm$^{-1}$) and $10^5$ Hz, respectively, was applied using a signal generator and an amplifier to the wet films during the process. The dielectric parameters were calculated as reported previously (*27*) using the root-mean-squared amplitude of the responding voltage ($V_m^*$) to the attenuated applied sinusoidal voltage ($V^*$) from the amplifier output, and the phase difference between $V^*$ and $V_m^*$. The capacitance and conductance of the sample were then calculated assuming a linear combination of the capacitance and conductance. A series of resistors with $R_k$ of 1000 Ω and $R_0$ of 1 Ω (or $R_k$ of 10 000 Ω and $R_0$ of 100 Ω) was used as a voltage divider so that the responding voltage was not larger than 1 V. Some waveforms of the applied voltage and the responding voltage were observed using a digital oscilloscope. In the case of a non-Ohmic response with a distorted waveform, a sinusoidal wave of the first order was extracted to give the values of the root-mean-squared amplitude and the phase difference in a lock-in amplifier.

The apparent dielectric constant, $\varepsilon_r'$, and loss factor, $\varepsilon_r''$, of the wet film during the process were also calculated as reported previously (*27*). In the present study, air and sufficiently dried hexane (*31*) were used for the calibration. For the calibration using hexane, the microdielectric sensor was completely immersed in the hexane-containing bottle. The dielectric parameters of 5CB were also measured similarly in the 5CB-containing bottle kept at 27°C.

The dielectric constant and loss factor of the solid films were also measured using an impedance analyser (*5*). The solid films were independently measured at a laboratory of TOSOH Analysis and Research Centre Co. The data independently measured were averaged.

The anisotropic textures were observed at room temperature using a polarised optical microscope with cross polarisers (Nikon, Eclipse E600W Pol) equipped with a CCD camera. The image data were recorded on a hard disk using a digital video recorder and transferred to a PC. For the observations of 5CB, room temperature was kept at 27°C.

## 3. Results and discussion

### *Electric field lines and molecular orientation of 5CB in the microdielectrometric measurement*

The electric field lines above our microdielectric sensor were calculated numerically, as discussed in Appendices A and B. Some results for the electric field lines are shown in Figure 1. Typical film thicknesses in the present study are also indicated in the figure by the solid, broken, and dotted lines. It is expected qualitatively that the long axes of a nematic liquid crystal with a positive dielectric anisotropy, such as 5CB, tend to orient locally along the electric field lines when the microdielectric sensor is completely immersed in the liquid crystal. At $x/D=0$, only the lateral component of the electric field contributes to the (whole) electric field, so that the lateral orientation of the long axes is expected to be significant around $x/D=0$. On the other hand, the orientation of the long axes is expected to be strongly dependent on the thickness of a thin layer, $z/D$, to which the liquid crystal is confined. As shown in Figure 1, most of the electric field lines around a thickness of $(d/D)_{1/2}$ are tilted with respect to the electrode surface and penetrate the thin layer. In addition, the electric field lines generated at $x/D$ from around $-0.7$ to $-0.5$ are confined within the thin layer, so that the long axes of the molecules within the region are expected to orient laterally. For a thicker layer with a thickness around $4(d/D)_{1/2}$, for instance, the region becomes wider, within which the electric field lines are confined. Consequently, the lateral orientation of the long axes is expected to be much more significantly found for the thicker layer. It should be noted that the electrostatic energy density at a given $x/D$ decreases with an increase in $z/D$, an example of which is discussed in Appendix A. In the present study, no specific modifications for molecular orientation were made on the surfaces of the microelectrodes. Therefore, it can be assumed that the lateral orientation in a layer for a nematic liquid crystal with a positive dielectric anisotropy is controlled by a competition between the behaviour of the electric field lines and the electrostatic energy density within the layer, other than the distortion free-energy density in the nematic phase as well as thermal agitation (*19*).

In the present study, the behaviour of the electric field lines was also investigated experimentally using a model liquid crystal 5CB via POM. A cell with a thickness (gap) around $(d/D)_{1/2}$, the gap of which was approximately 30 μm, was prepared using a microdielectric sensor (bottom) and a slide glass (top) with a polyimide film as a spacer, and 5CB in the isotropic phase was injected into the cell by capillary force. In addition, the anisotropic textures of 5CB on a pair of the microelectrodes were observed for a layer with a thickness around $2(d/D)_{1/2}$, the surface of which was free and adjacent to the air atmosphere and the thickness of which was approximately 60 μm.

In figure 2, captured images during observations with a polarised optical microscope are shown for a 5CB layer, confined in the cell with a gap of approximately 30 μm under no electric field, and under the sinusoidal electric field with different amplitudes and frequency of $10^5$ Hz. The images on the right were taken so that the lines of the electrode edges were located approximately 45° with respect to the polarising direction. (The images on the right were taken after observations of the images on the left, because the electric field was applied during the observation. Therefore, the texture on the right at a given amplitude does not correspond in detail to that on the left. The images shown in Figure 3 were observed similarly.) In the cell, multi-domains with disclinations of 5CB are found under no electric field, as shown in Figure 2(a) (left and right). Similar textures are found in the images taken under the electric field with small amplitudes of 0.05 and 0.2 kV mm$^{-1}$ (Figures 2(b) and 2(c)). In Figures 2(d)–2(f), significantly different textures are found with interference colours, suggesting the tilted orientation of the long axes along the electric field lines shown in Figure 1. Furthermore, a characteristic texture showing a lateral orientation is clearly found around the region between the electrodes. In Figure 2(f) (right), a relatively homogeneous region suggesting a lateral orientation is spread beyond the gap between the electrodes, and it is much wider than the expectation based on the electric field lines shown in Figure 1.

Captured images similar to those in Figure 2 are shown in Figure 3 for a 5CB layer on a pair of the microelectrodes with a thickness of approximately 60 μm. For the thicker layer, the lateral orientation can

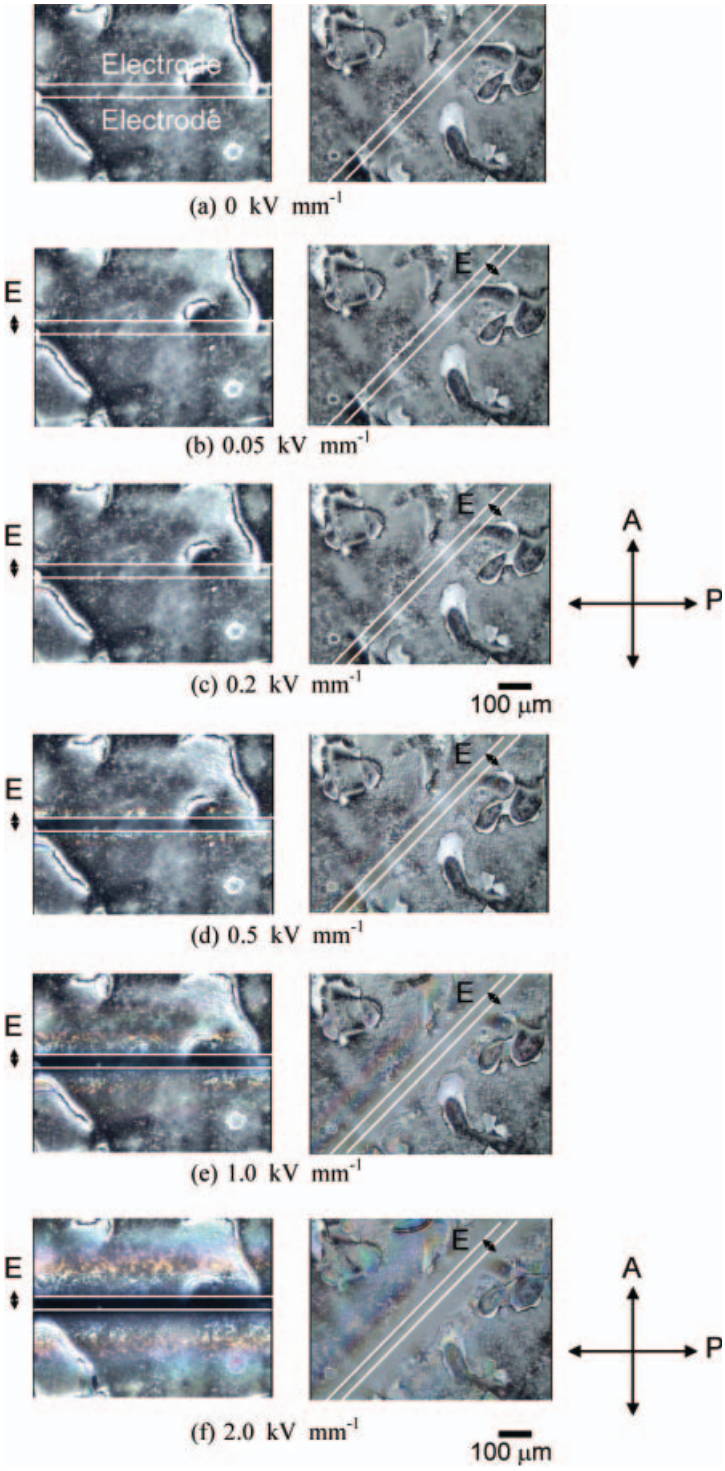


Figure 2. Captured images observed using a polarised optical microscope for a 5CB layer on a pair of the microelectrodes, which was confined in a cell kept at 27°C, with a gap of approximately 30 μm (a) under no electric field and under the sinusoidal electric field with amplitudes of (b) 0.05 kV mm$^{-1}$, (c) 0.2 kV mm$^{-1}$, (d) 0.5 kV mm$^{-1}$, (e) 1.0 kV mm$^{-1}$ and (f) 2.0 kV mm$^{-1}$. The frequency of the electric field was $10^5$ Hz. The images on the right were taken so that the electrode edges were located approximately 45° relative to the polarising direction.

be found much more easily in the image taken under an electric field of 0.2 kV mm$^{-1}$, as shown in Figure 3(b). The region suggesting the lateral orientation found in Figure 3(e) (right) is significantly wider than that found in Figure 2(f) (right). In addition, textures with interference colours similar to those shown in Figure 2 can

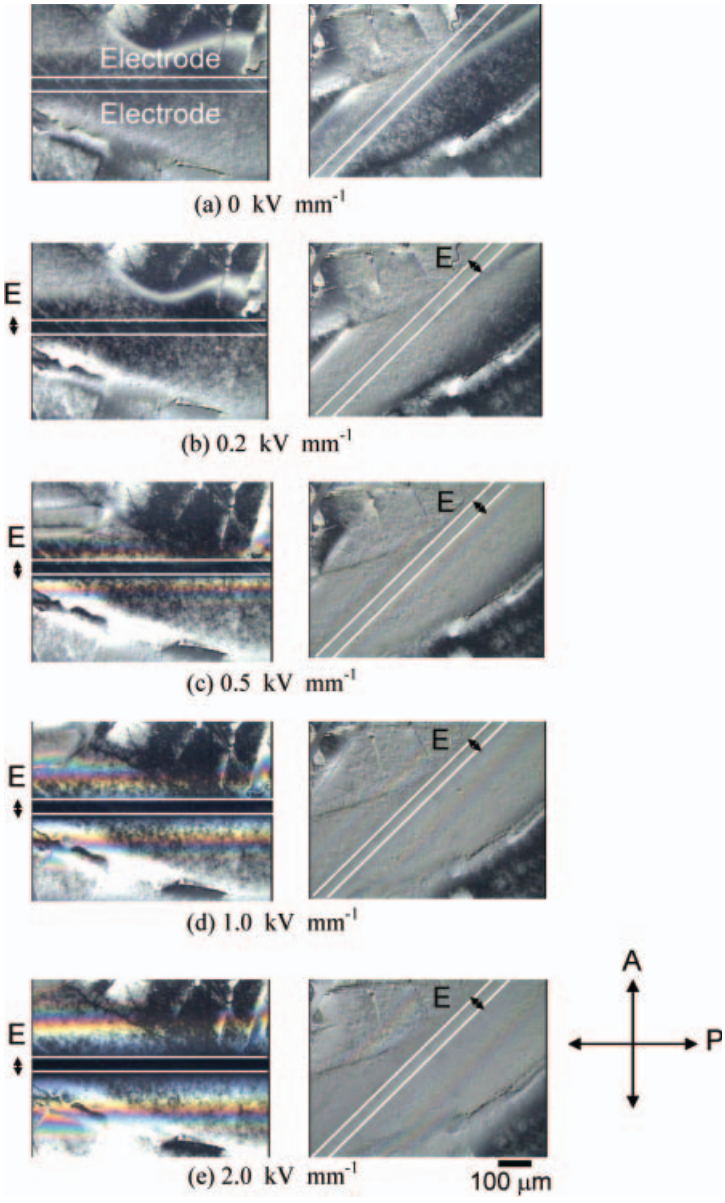


Figure 3. Captured images similar to Figure 2 for a 5CB layer on a pair of the microelectrodes, the surface of which was free and adjacent to the air atmosphere kept at 27°C, with a thickness of approximately 60 μm (a) under no electric field and under the sinusoidal electric field with amplitudes of (b) 0.2 kV mm$^{-1}$, (c) 0.5 kV mm$^{-1}$, (d) 1.0 kV mm$^{-1}$ and (e) 2.0 kV mm$^{-1}$. The frequency of the electric field was $10^5$ Hz.

be clearly seen in Figures 3(c)–3(e). Therefore, the long axes of 5CB within the thin layer on the order of $(d/D)_{1/2}$ tend to orient along the electric field lines, whereas those within the thicker layer with a thickness around $2(d/D)_{1/2}$ basically orient along the electric field lines but also preferentially orient laterally under the electric field. The lateral orientation may be much more significantly emphasised in the thicker layer, whereas it is expected that the orientation of the long axes is suppressed by the decrease in the electrostatic energy density along the layer normal. The portion of randomly oriented multi-domains in a sufficiently thicker layer is considered to be negligible for the dielectric measurement, such as the case for the microelectrodes completely immersed in the 5CB-containing bottle. The measured dielectric constants of 5CB are discussed below.

The measured dielectric constants, $<\varepsilon_r'>$ and $<\cos^2\theta>$, calculated using equation (1), for 5CB are plotted in Figure 4 against the amplitude of the electric field of $10^5$ Hz. The dielectric constants, $\varepsilon_{//}$ and $\varepsilon_\perp$, which were measured at a frequency on the order of $10^3$ Hz and reasonably assumed to be static (*29*), and the average $\varepsilon_m=(\varepsilon_{//}+2\varepsilon_\perp)/3$ are shown by

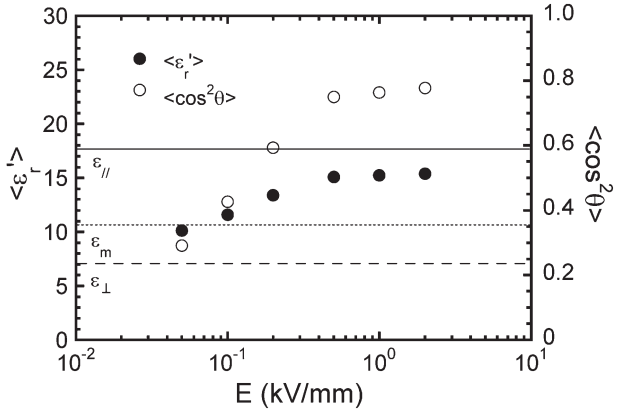


Figure 4. The measured dielectric constant, $<\varepsilon_r'>$, and $<\cos^2\theta>$, calculated using equation (1), for 5CB plotted against the amplitude of the sinusoidal electric field with a frequency of $10^5$ Hz. The microdielectric sensor was completely immersed in the 5CB-containing bottle kept at 27°C. The dielectric constants $\varepsilon_{//}$, $\varepsilon_\perp$, which were measured at a frequency on the order of $10^3$ Hz (*29*), and the average $\varepsilon_m=(\varepsilon_{//}+2\varepsilon_\perp)/3$ are shown by the solid line, broken line and dotted line, respectively.

solid, broken and dotted lines, respectively. In the present study, the dielectric constant was measured at a frequency of $10^5$ Hz. The relaxation time of the longitudinal rotation, $\tau_{//}$, for 5CB was reported to be around $2.9\times10^{-8}$ s, which was measured at 303 K and a pressure of 0.1 MPa (*30*). Therefore, the relaxation frequency at 300 K was estimated to be in the several megahertz range. Although the dielectric parameters at $10^5$ Hz may be slightly affected by the dielectric relaxation, the dielectric constant measured at $10^5$ Hz is well assumed to be the static dielectric constant. In Figure 4, the dielectric constant, $<\varepsilon_r'>$, measured at a small amplitude of 0.05 kV mm$^{-1}$ is nearly equal to or slightly smaller than the average $\varepsilon_m$, corresponding to a multi-domain texture shown in Figure 2 at the same amplitude. The measured dielectric constant initially increases continuously without showing a threshold amplitude, and it increases only slightly at larger amplitudes. Correspondingly, $<\cos^2\theta>$ increases in a manner similar to $<\varepsilon_r'>$, reaching a value of 0.8 at 2.0 kV mm$^{-1}$. The increase in $<\varepsilon_r'>$ (or $<\cos^2\theta>$) is quite consistent with the increase in the region for the lateral orientation observed in Figure 3.

### *Microdielectrometric monitoring of film preparation process for HPC during casting under the sinusoidal electric field with large amplitude*

In the present study, the microdielectrometric monitoring was also performed for the preparation process of a solid film cast from an isotropic aqueous solution of 30 wt % HPC under the sinusoidal electric field of large amplitude. The measured dielectric constant, $<\varepsilon_r'>$, and loss factor, $<\varepsilon_r''>$, divided by $J_{14}(d_D/D)$ for normalisation are shown in Figure 5 for the wet films with different film thicknesses during the casting process. The measured dielectric loss factor, $<\varepsilon_r''>$, is also considered as the energy-density average over the volume pervaded by the electric field. In the case of 5CB, as discussed above, the parameters $\varepsilon_{//}$ and $\varepsilon_\perp$ in Equation (1) are known in the nematic phase, and a constant volume (as well as concentration) may be assumed. Therefore, the parameter $<\cos^2\theta>$ can be estimated based on Equation (1). In contrast, the phase of the HPC solution during the casting process was drastically changed from isotropic phase to solid phase via its liquid crystalline phase, and the parameters analogous to Equation (1) cannot be determined. Further study is needed to discuss the problem in detail.

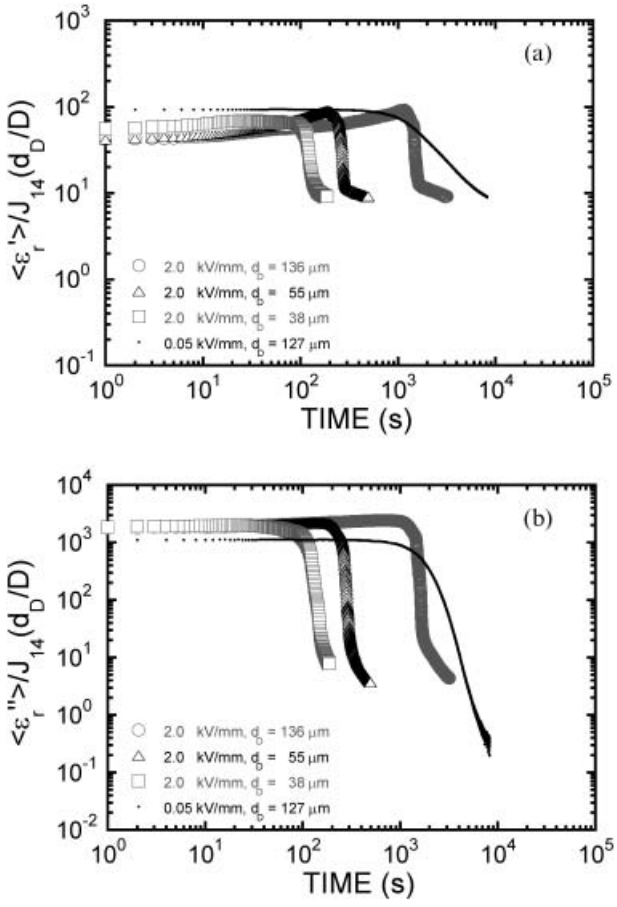


Figure 5. (a) The measured dielectric constant and (b) loss factor for the HPC solutions during the casting process under the sinusoidal electric field. The two parameters were divided by $J_{14}(d_D/D)$ calculated in Appendix A. The frequency of the electric field was $10^5$ Hz. The amplitude and the thickness of the solid films $d_D$ are shown.

In Figure 5, the initial values of $<\varepsilon_r'>/J_{14}(d_D/D)$ [or $<\varepsilon_r''>/J_{14}(d_D/D)$] measured at $2.0\,kV\,mm^{-1}$ are mostly identical for different film thicknesses but slightly smaller (or larger) than that measured at $0.05\,kV\,mm^{-1}$. It is considered that the slight differences are caused by the non-Ohmic conduction at the larger amplitude of the electric field; in this case higher order harmonics in the slightly distorted waves of the responding current were removed. It is worthwhile to note that $<\varepsilon_r'>/J_{14}(d_D/D)$ measured at $2.0\,kV\,mm^{-1}$ for a layer of the solution initially increases gradually, showing a maximum and decreasing steeply, then gradually decreases in Figure 5(a). The behaviour of $<\varepsilon_r'>/J_{14}(d_D/D)$ is considerably different to that measured at $0.05\,kV\,mm^{-1}$.

Furthermore, POM simultaneously applied to the microdielectrometry showed that macroscopic and relatively homogeneous textures with optical anisotropy were developed around the electrodes at times around the maxima shown in Figure 5(a) under the electric field of $2.0\,kV\,mm^{-1}$. In Figure 6, typical images are shown. The electrode edges were set in the direction approximately 45° relative to the polarising direction. The observations were not easy, especially for the thinner layers, without a 530 nm retarder. In addition, the field of view became much darker for the textures developed under the electric field of $2.0\,kV\,mm^{-1}$ at times after the steep decrease shown in Figure 5(a). Correspondingly, it is considered that diffusive molecular motions (or fluctuations of director) inducing a possible light scattering were substantially suppressed because the HPC in the layers became quite concentrated. (The brightness and contrast of the images in Figures 6(a) and 6(c) (and Figures 9 and 10 shown later) were digitally enhanced in a similar manner, so that qualitative comparison with these images is not affected by the enhancement.)

The image for the $d_D$ of 55 μm, which was observed with the 530 nm retarder, is shown in Figure 6(b). Similar images near the termination of the casting process are also shown in Figure 7. It is of great interest that the orientation of anisotropic domains has been induced by the sinusoidal electric field of $2.0\,kV\,mm^{-1}$, whereas a randomly oriented polydomain texture was found under the electric field of $0.05\,kV\,mm^{-1}$ (*27*). For the image of the thicker layer shown in Figure 6(c), the anisotropic texture is fairly homogeneous and spread widely across the field of view. Further, the interference colour shown in Figure 6b shows that the sign of the retardance for the HPC layer is positive, because the interference colour is slightly blue-shifted from the sensitive colour of the retarder of 530 nm on a scale of Newton's colour sequence (*32*). The observed retardance for the HPC layer contributes additively to the retardance of 530 nm in the geometry. A similar blue-shift was seen for other layers with a $d_D$ of 38 and 136 μm and can also be seen in the images shown in Figure 7 near the termination of the casting process.

On the basis of relationship between the average molecular orientation and the birefringence under shear flow reported so far (*33, 34*), the long axis of HPC tends to orient along the slow axis Z′ of the retarder in the present study. The flow birefringence study on anisotropic solutions of HPC showed that the birefringence oriented along the flow direction, which was determined with the polariser and analyser oriented at 45° with respect to the flow, was positive and increased with the shear rate (*33*). Furthermore, an in-situ X-ray scattering study on sheared anisotropic solutions of HPC also showed that the HPC chain segments were preferentially oriented parallel to the shear direction (*34*). Therefore, the long axis of HPC is considered to orient approximately along the shear direction in the anisotropic solutions.

In the present study, it is considered that the orientation of anisotropic domains perpendicular to the electric field reported for liquid crystals of small molecules (*19, 20*) was also induced in the HPC solutions during casting from an isotropic aqueous solution by application of the large amplitude of an electric field of $10^5$ Hz. It can be assumed that the dielectric anisotropy was negative at this frequency. It is additionally expected that the longitudinal rotation was relaxed, whereas the transversal rotational diffusion of a partially flexible rod was still active for the HPC molecules with side chains as well as a local motion of chain segments confined in the concentrated solution (*5*). The transversal rotation of an HPC molecule was then induced by the electric field and an angular momentum about the long axis was also induced, giving a steady state for the long axis after a transient precession. Consequently, the long axis tended to orient perpendicular to the electric field, the direction of which is also parallel to the slow axis Z′ of the retarder shown in Figures 6 and 7.

In addition, the distribution of the blue-shifted interference colour shown in Figure 7 is dependent on the layer thickness. For the layer with a $d_D$ of 38 μm, the blue-shifted colour is seen around the electrodes, including the gap between them. However, a slightly shallow colour within the gap between the electrodes can be found for the layer with a $d_D$ of 55 μm, and the colour is spread fairly widely across the field of view for the layer with a $d_D$ of 136 μm, the results of which are closely related to the distribution of the electrostatic energy density above the microelectrodes.

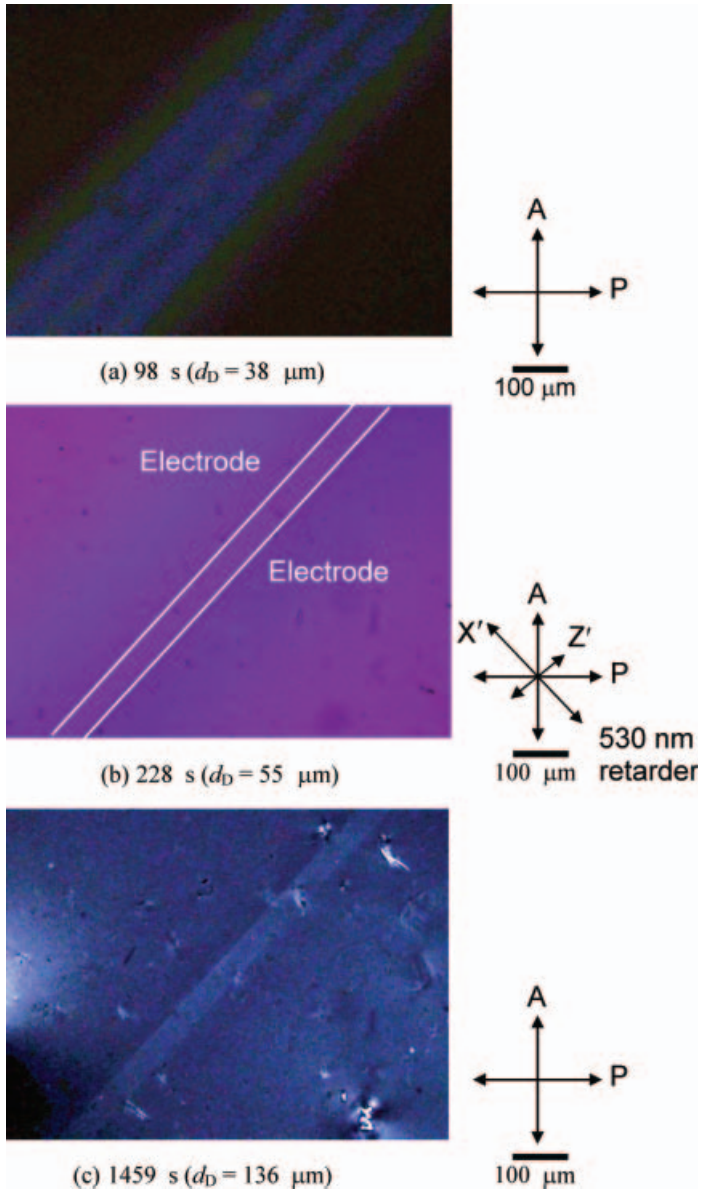


Figure 6. Captured images observed using a polarised optical microscope for the HPC solutions during casting under the sinusoidal electric field of 2.0 kV mm$^{-1}$ at a time of (a) 98 s for $d_D$=38 μm, (b) 228 s for $d_D$=55 μm and (c) 1459 s for $d_D$=136 μm. The electrode edges were located approximately 45° relative to the polarising direction. Image (b) was observed with a 530 nm retarder, the slow axis, Z′, of which is indicated.

***Comparison of relations between the normalised dielectric constant and loss factor of film preparation process for HPC during casting under the sinusoidal electric field with small and large amplitudes and development of the film textures thereafter***

In Figure 8, the logarithmic relations between $\varepsilon_r''/J_{14}(d_D/D)$ and $\varepsilon_r'/J_{14}(d_D/D)$ measured at 2.0 kV mm$^{-1}$ are plotted for the dielectric parameters shown in Figure 5. The logarithmic relation between the two parameters measured at 0.05 kV mm$^{-1}$ is also plotted. In Figure 8, the two parameters measured at 2.0 kV mm$^{-1}$ are superposed on a single curve, the superposition behaviour of which is similar as reported for the parameters measured at 0.05 kV mm$^{-1}$ (*27*). However, the curve for 2.0 kV mm$^{-1}$ is considerably different to that for the polydomain texture found under the electric field of 0.05 kV mm$^{-1}$. The curve for 2.0 kV mm$^{-1}$ initially increases and then decreases. At the same time, macroscopic orientation of the HPC molecules was observed during the casting process, as shown in Figures 6 and 7. In contrast, the curve for 0.05 kV mm$^{-1}$ monotonically decreases showing a randomly oriented polydomain texture during the process.

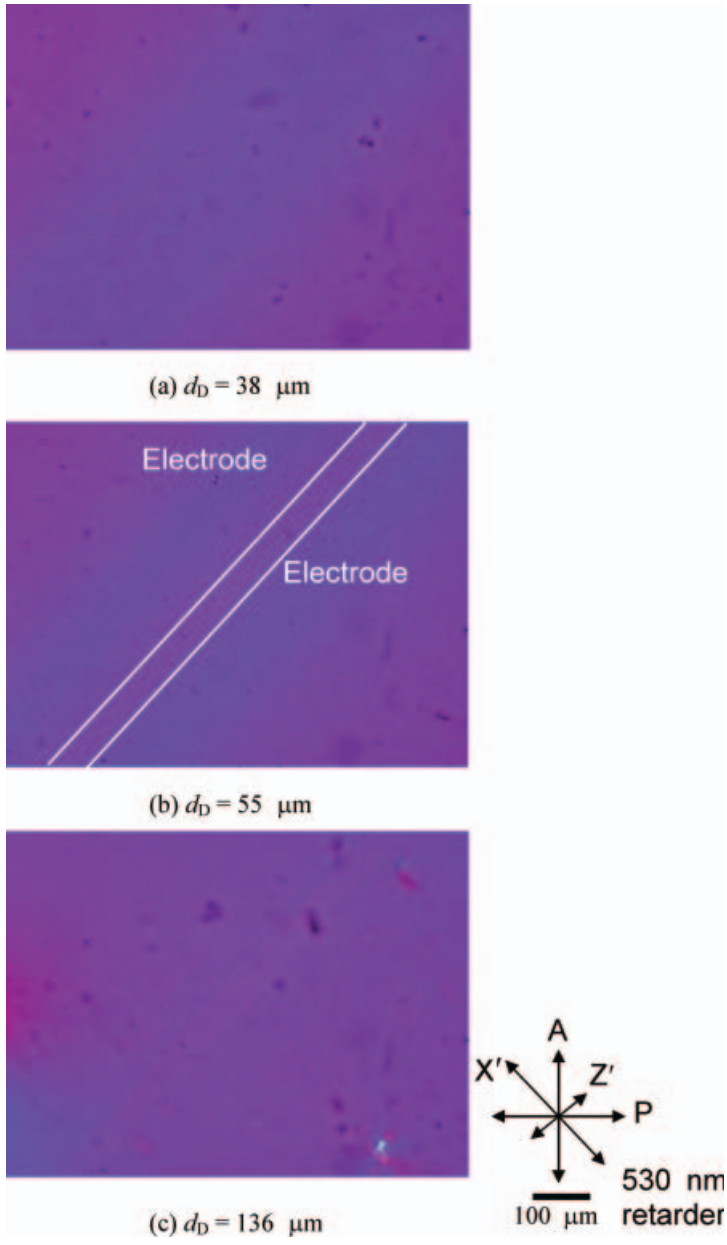


Figure 7. Captured images near the termination of the casting process under the sinusoidal electric field of 2.0 kV mm$^{-1}$ observed using a polarised optical microscope with a 530 nm retarder for the HPC films for (a) $d_D$=38 μm, (b) $d_D$=55 μm and (c) $d_D$=136 μm. The directions of the electrode edges and the slow axis Z′ of the retarder were similarly set as shown in Figure 6.

As discussed already, the measured dielectric constant for 5CB with a positive dielectric anisotropy increased with the long axis of 5CB oriented along the electric field lines. It is expected for the HPC solution during casting that the dielectric parameter $\varepsilon_r'/J_{14}(d_D/D)$ measured under the electric field of 2.0 kV mm$^{-1}$ is determined by a competition between the removal of the water solvent and the orientation of HPC domains. Therefore it is considered that the orientation was a dominant effect at the initial stage of the casting process on $\varepsilon_r'/J_{14}(d_D/D)$ over the removal of water solvent.

In addition, the parameter $\varepsilon_r''/J_{14}(d_D/D)$ for 2.0 kV mm$^{-1}$ shown in Figure 8 is much larger than that for 0.05 kV mm$^{-1}$ at a given $\varepsilon_r'/J_{14}(d_D/D)$, suggesting that the larger $\varepsilon_r''/J_{14}(d_D/D)$ was closely related to the non-Ohmic conduction. Near the termination of the process, however, the responding current became weak so that experimental errors were not negligible and such results are not plotted in Figure 8. Instead, the dielectric parameters for sufficiently dried films with the oriented texture and polydomain texture were also measured using an

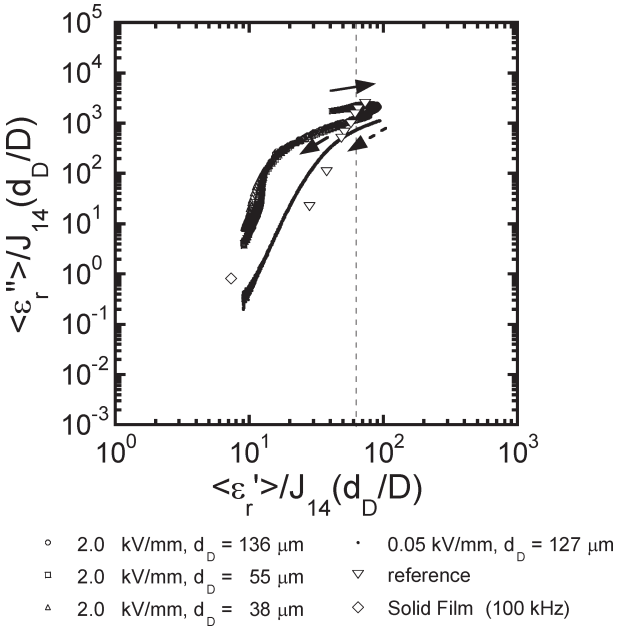


Figure 8. The logarithmic relations between $<\varepsilon_r''>/J_{14}(d_D/D)$ and $<\varepsilon_r'>/J_{14}(d_D/D)$ shown in Figure 5. The data for solutions above 30 wt % HPC measured with a liquid cell (*5*) and the solid film are also plotted. The broken line represents the value of the relative dielectric constant for the onset of the mesophase formation reported previously (*5*).

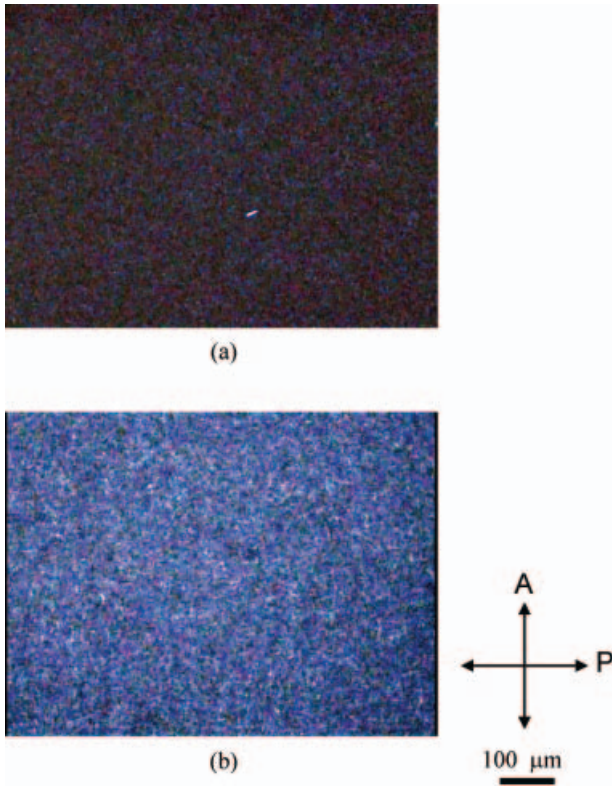


Figure 9. Captured images observed using a polarising optical microscope for the HPC solid film with a $d_D$ of 59 μm cast under the sinusoidal electric field of 0.05 kV mm$^{-1}$ (a) as prepared and (b) kept at room temperature.

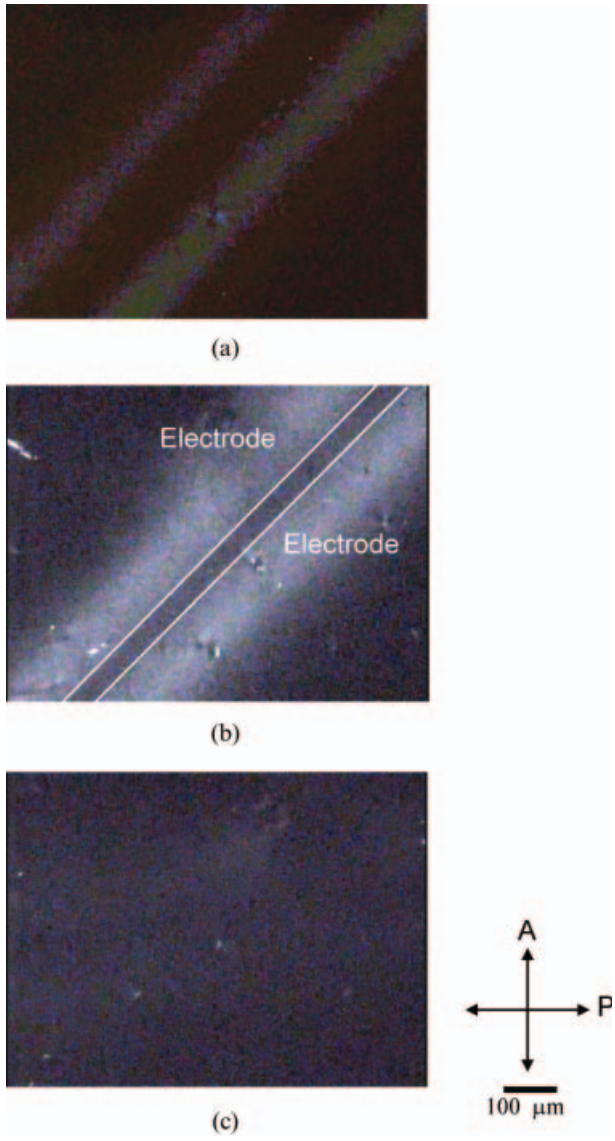


Figure 10. Captured images similar to Figure 9 for the HPC solid film with a $d_D$ of 55 μm cast under the sinusoidal electric field of 2.0 kV mm$^{-1}$ (a) as prepared, (b) and (c) kept at room temperature. Image (c) was taken after that of (b) with a clockwise rotation of 45° on the stage.

impedance analyser (HP, 4192A), but no remarkable differences were found between the sufficiently dried films. Although the absolute values may not be accurately measured, it is strongly suggested that even a small amount of water solvent plays a significant role in the dielectric parameters during the process. A significant effect of a small amount of water was also reported by Shinouda and Moteleb on the dielectric properties for HPC solid films (*9*). It can also be considered that even a small amount of water solvent acted as an effective probe for the microdielectrometric monitoring in the present study.

Finally, the textures of the solid films were found to be developed when they were kept at room temperature. In Figure 9, captured images observed using a polarised optical microscope are shown for the HPC solid film with a $d_D$ of 59 μm cast under the electric field of $0.05\,kV\,mm^{-1}$ as prepared (Figure 9(a)), and kept at room temperature for several months (Figure 9(b)).

Similar images are also shown in Figure 10 for the HPC solid film with a $d_D$ of 55 μm cast under the electric field of $2.0\,kV\,mm^{-1}$ as prepared (Figure 10(a)), and kept at room temperature for several months (Figures 10(b) and 10(c)). The image in Figure 10c was taken after that of Figure 10b with a clockwise rotation of 45° on the stage. Interestingly, both the randomly oriented polydomain texture and the oriented domains were developed at room temperature keeping their texture as prepared. Especially, no remarkable relaxation of the oriented domains is found in Figure 10b. In addition, extinction is observed in Figure 10c, showing that no remarkable relaxation for the long axes of the HPC molecules was induced at room temperature. It is considered that the development of the textures kept at room temperature was induced by molecular motions closely related to secondary dispersions for the HPC solid films found in the dielectric spectroscopy.

## 4. Conclusions

In the present study, microdielectrometry was applied to macroscopically anisotropic media. In the first place, the distribution and effective portion of the electrostatic energy density, $w_{14}$ and $J_{14}$, respectively, were calculated taking into account the additive contributions of four pairs of our microelectrodes. The electric field lines were also calculated numerically, and the behaviour was investigated experimentally with POM using thin layers of a nematic liquid crystal, 4,4′-*n*-pentylcyanobiphenyl (5CB), with a positive dielectric anisotropy. The long axes of 5CB within the thin layer on the order of the penetration depth of the electrostatic energy density $(d/D)_{1/2}$ tended to orient along the electric field lines, whereas those within the thicker layer with a thickness around $2(d/D)_{1/2}$ basically oriented along the electric field lines but also preferentially oriented laterally under the electric field. The measured dielectric constant, $<\varepsilon_r'>$, initially increased continuously without a threshold amplitude, and later only slightly with an increase in the amplitude of the electric field. The orientation parameter, $<\cos^2\theta>$, along the electric field lines increased in a manner similar to that for $<\varepsilon_r'>$, reaching a value of 0.8 at $2.0\,kV\,mm^{-1}$. The increase in $<\varepsilon_r'>$ was quite consistent with the increase in the region for the lateral orientation.

Secondly, microdielectrometric monitoring has been reported for the preparation process of a solid film with oriented domains cast from an isotropic aqueous solution of HPC under the sinusoidal electric field with amplitude and frequency of $2.0\,V\,\mu m^{-1}$ ($kV\,mm^{-1}$) and $10^5$ Hz, respectively. It is worth noting that the normalised dielectric constant, $<\varepsilon_r'>/J_{14}(d_D/D)$, for a layer of the solution measured at $2.0\,kV\,mm^{-1}$ showed an initial increase with a maximum, with subsequent steep and gradual decreases, the behaviour of which was much different from that measured at $0.05\,kV\,mm^{-1}$. It is of great interest that the macroscopic orientation of anisotropic domains was induced during casting even from an isotropic aqueous solution by the electric field of $2.0\,kV\,mm^{-1}$. The orientation of the long axis was considered to be perpendicular to the electric field, at the frequency of which the dielectric anisotropy was assumed to be negative, and the longitudinal rotation of the rod-like molecules was relaxed whereas transversal rotation was still active. In the logarithmic relation between the normalised dielectric constant and loss factor, $<\varepsilon_r''>/J_{14}(d_D/D)$, the two parameters measured for different film thicknesses at $2.0\,kV\,mm^{-1}$ were superposed on a single curve. The curve for electrically oriented domains was considerably different to that for a randomly oriented polydomain texture found under the electric field of $0.05\,kV\,mm^{-1}$. The different trajectories of the curves can be effective for the in-situ monitoring of the macroscopic orientation of a film during casting. In addition, the textures of the solid films were found to be developed keeping their texture as prepared even when they were kept at room temperature.

## Acknowledgments

This work was partially supported by a Grant-in-Aid for Scientific Research from the Japan Society for the Promotion of Science. We are also grateful to Dr. Shimura (TOSOH Analysis and Research Centre Co.) for the dielectric measurements of the solid films.

## References

(1) Werbowyj R.S.; Gray D.G. *Mol. Cryst. Liq. Cryst.* **1976**, *34*, 97–103.
(2) Werbowyj R.S.; Gray D.G. *Macromolecules* **1980**, *13*, 69–73.
(3) Conio G.; Bianchi E.; Ciferri A.; Tealdi A.; Aden M.A. *Macromolecules* **1983**, *16*, 1264–1270.
(4) Fried F.; Sixou P. *J. Polym. Sci. Polym. Chem. Ed.* **1984**, *22*, 239–247.
(5) Tanaka K.; Morina T.; Tanabe Y.; Akiyama R. *Liq. Cryst.* **2007**, *34*, 1019–1028.
(6) Guido S. *Macromolecules* **1995**, *28*, 4530–4539.
(7) Samuels R.J. *J. Polym. Sci. A*-2 **1969**, *7*, 1197–1258.

(8) Moteleb M.M.A.; Naoum M.M.; Shalaby M.M.; Saad G.R. *Polym. Int.* **1994**, *34*, 363–367.
(9) Shinouda H.G.; Moteleb M.M.A. *J. Appl. Polym. Sci.* **2005**, *98*, 571–582.
(10) Meißner D.; Einfeldt J.; Kwasniewski A. *J. Non-Crystalline Solids* **2000**, *275*, 199–209.
(11) Pizzoli M.; Scandola M.; Ceccorulli G. *Plast. Rubber Composites Process. Appl.* **1991**, *16*, 239–244.
(12) Rachocki A.; Markiewicz E.; Tritt-Goc J. *Acta Phys. Polon. A* **2005**, *108*, 137–145.
(13) Riti J-B.; Navard P. *J. Rheol.* **1998**, *42*, 225–237.
(14) Tanaka K.; Yonetake K.; Masuko T.; Akiyama R. *J. Macromol. Sci. B* **2003**, *42*, 901–914.
(15) Tanaka K.; Akiyama R.; Takada K. *J. Appl. Polym. Sci.* **1997**, *66*, 1079–1084.
(16) Block H.; Shaw C.P. *Polymer* **1992**, *33*, 2459–2462.
(17) Martin D.C. *Polymer* **2002**, *43*, 4421–4436.
(18) Yen C.-C.; Araoka F.; Tokita M.; Kawauchi S.; Park B.; Takezoe H.; Watanabe J. *Jap. J. Appl. Phys.* **2004**, *43*, 7026–7031.
(19) De Gennes P.G.; Prost J. *The Physics of Liquid Crystals,* 2nd ed, Clarendon Press: Oxford, 1993; Chapters 3 and 6.
(20) Haas W.; Adams J.; Flannery J.B. *Phys. Rev. Lett.* **1970**, *24*, 577–578.
(21) Aronson C.L.; Catalogna J.C.; Webster W.D. *Polym. Bull.* **2004**, *53*, 43–52.
(22) Sheppard N.F.; Day D.R.; Lee H.L.; Senturia S.D. *Sensors Actuators* **1982**, *2*, 263–274.
(23) Senturia S.D.; Sheppard N.F. Jr.; Lee H.L.; Day D.R. *J. Adhesion* **1982**, *15*, 69–90.
(24) Eloundou J.P.; Ayina O.; Nga H.N.; Gerard J.F.; Pascault J.P.; Boiteux G.; Seytre G. *J. Polym. Sci. B* **1998**, *36*, 2911–2921.
(25) Fodor J.; Hill D.A. *Macromolecules* **1992**, *25*, 3511–3520.
(26) Fodor J.S.; Hill D.A. *J. Rheol.* **1994**, *38*, 1071–1100.
(27) Tanaka K.; Tanabe Y.; Morina T.; Akiyama R. *Liq. Cryst.* **2008**, *35*, 253–264.
(28) Harvey B., *Computer Science Logo Style, Vol. 1. Intermediate Programming;* MIT Press: 1985.
(29) Dunmur D.A.; Manterfield M.R.; Miller W.H.; Dunleavy J.K. *Mol. Cryst. Liq. Cryst.* **1978**, *45*, 127–144.
(30) Kreul H.-G.; Urban S.; Würflinger A. *Phys. Rev. A* **1992**, *45*, 8624–8631.
(31) Weast R.C. (Ed.), *CRC Handbook of Chemistry and Physics,* 57th ed.; CRC Press: Cleveland, OH, 1976–1977.
(32) Larson R.G.; Mead D.W. *Liq. Cryst.* **1992**, *12*, 751–768.
(33) Hongladarom K.; Secakusuma V.; Burghardt W.R. *J. Rheol.* **1994**, *38*, 1505–1523.
(34) Keates P.; Mitchell G.R.; Peuvrel-Disdier E.; Navard P. *Polymer* **1993**, *34*, 1316–1319.



## Appendix A

The distribution and effective portion of the electrostatic energy density for the microelectrodes, which were simply calculated halfway between the electrodes above the surface, were reported previously (*27*). In the present study, both the lateral and vertical components of the electric field, $E_x(x, z)$ and $E_z(x, z)$, respectively, were investigated, taking into account the additive contributions of four pairs of the electrodes shown in Figure A1a. Considering the dimensions of the microelectrodes, the electric field can be assumed to be two-dimensional. The electrodes on the $x$–$z$ plane, part of which is shown in Figure A1b, can also be assumed to be four pairs of line charges of length $W$ with charge densities $\lambda$ and $-\lambda$. The lateral and vertical components of the electric field are simply calculated as follows:

$$E_x(x,z) = \frac{\lambda}{4\pi\varepsilon_0 D}\sum_{i=1}^{4}(-1)^{i-1}\left[\frac{1}{\sqrt{(x/D-A_i)^2+(z/D)^2}}+\frac{1}{\sqrt{(x/D+A_i)^2+(z/D)^2}}-\frac{1}{\sqrt{(x/D-B_i)^2+(z/D)^2}}-\frac{1}{\sqrt{(x/D+B_i)^2+(z/D)^2}}\right], \quad \text{(A1)}$$

$$E_z(x,z) = \frac{\lambda}{4\pi\varepsilon_0 D}\sum_{i=1}^{4}(-1)^{i-1}\left[-\frac{x/D-A_i}{\sqrt{(x/D-A_i)^2+(z/D)^2}}-\frac{x/D+A_i}{\sqrt{(x/D+A_i)^2+(z/D)^2}}+\frac{x/D-B_i}{\sqrt{(x/D-B_i)^2+(z/D)^2}}+\frac{x/D+B_i}{\sqrt{(x/D+B_i)^2+(z/D)^2}}\right], \quad \text{(A2)}$$

$$A_i = (2i-1)/2+(i-1)W/D, \quad \text{(A3)}$$

$$B_i = (2i-1)/2+iW/D, \quad \text{(A4)}$$

where $\varepsilon_0$ is the permittivity of free space and $D$ is the gap distance between the electrodes of the nearest neighbours.

The distribution of the electrostatic energy density $w_{14}$ halfway between the electrodes above the surface was calculated based on $E_x(0, z)$:

$$w_{14}(0,z) = [E_x(0,z)]^2 \Big/ \int_0^\infty [E_x(0,z)]^2 dz \equiv w_{14}(z/D) \quad \text{(A5)}$$

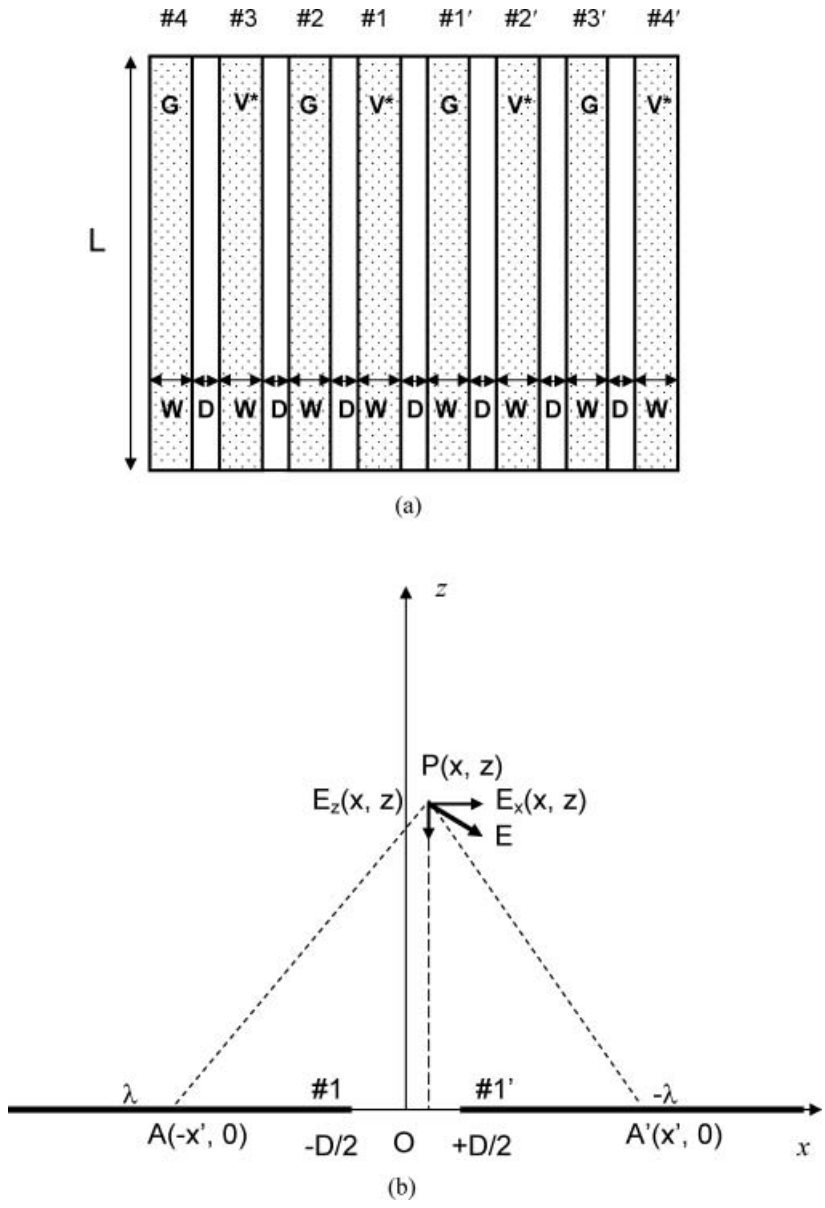


Figure A1. (a) Schematic illustrations of the top view of the transparent interdigitated electrodes deposited on a glass substrate, and (b) the side view of part of electrodes #1 and #1′. In (a), four pairs of electrodes with the width $W$ and length $L$ for high voltage ($V$*) and ground ($G$) are numbered. The gap distance between the electrodes of the nearest neighbours is denoted by $D$. The ratio in the figure is not faithfully reproduced.

In the present paper, $w_{14}$ was calculated numerically with a (dimensionless) parameter $\zeta=z/D$. The numerical integration in equation (A5) was made from $\zeta=0$ to $\zeta=100$ with the initial value of zero and $\Delta\zeta=0.01$. The integration to $\zeta=100$ would practically be regarded as that to infinity because the values of the integral were almost saturated around $\zeta=10$.

Similarly, an effective portion of the electrostatic energy density $J_{14}$ was also calculated numerically:

$$J_{14}(0,z)=\int_0^{+z} w_{14}(0,z)dz \equiv J_{14}(z/D). \qquad \text{(A6)}$$

In Figure A2, $w_{14}/(1/D)$ and $J_{14}$ are plotted against $z/D$, comparing $w/(1/D)=(4/\pi)[1+4(z/D)^2]^{-1}$ and $J=(2/\pi)\tan^{-1}(2z/D)$ reported previously (*27*), the calculations in which only a pair of electrodes #1 and

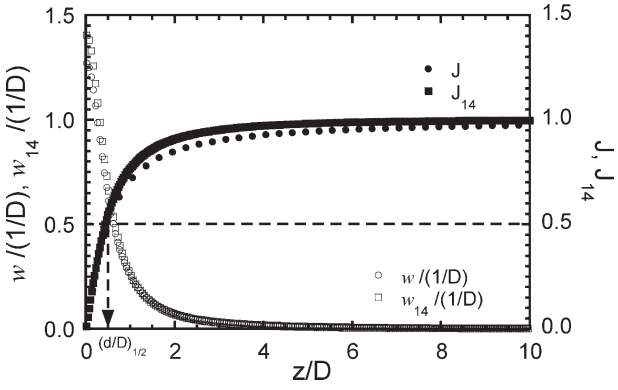


Figure A2. The distribution and effective portion of the electrostatic energy density $w_{14}/(1/D)$ and $J_{14}$, respectively, plotted against $z/D$, the calculations in which the additive contributions of four pairs of electrodes shown in Figure A1a were taken into account. The two parameters are compared with $w/(1/D)$ and $J$ reported previously (*27*), considering only a pair of semi-infinite planes of electrodes #1 and #1′.

#1′ assuming a pair of semi-infinite planes, was taken into account. The errors estimated from $(J_{14}-J)/J_{14}$ were less than 10%.

## Appendix B

In the present study, the electric field lines are also calculated numerically based on equations (A1)–(A4) shown in Appendix A using an algorithm of Turtle Graphics (*28*). Applying the algorithm, the electric field lines are calculated stepwise. At first, the unit stroke $\Delta l$ was set to be a constant. For the initial condition, a position $Q_0(\xi_0, \zeta_0)$ was given above the electrode #1 in close proximity. The lateral and vertical components of the electric field, $E_x(\xi_0, \zeta_0)$ and $E_z(\xi_0, \zeta_0)$, respectively, were calculated using equations (A1)–(A4). The direction $\phi_0$ was then calculated as follows:

$$\phi_0 = \tan^{-1}[E_z(\xi_0,\zeta_0)/E_x(\xi_0,\zeta_0)], \tag{A7}$$

where all the parameters $\Delta l$, $\xi_0$ and $\zeta_0$ are dimensionless and scaled by $D$.

The next position $Q_1(\xi_1, \zeta_1)$ was determined according to the following equations:

$$\xi_1 = \xi_0 + \Delta l \cos\phi_0, \tag{A8}$$

$$\zeta_1 = \zeta_0 + \Delta l \sin\phi_0. \tag{A9}$$

The calculations using equations similar to those (A7)–(A9) were repeated until the position $Q_n(\xi_n, \zeta_n)$ ($n=0, 1, 2, ...$) was sufficiently close to electrode #1′, or sufficiently away from electrode #1. A line of the electric field can be calculated as a trace of positions $Q_n$'s. In the present study, both $\Delta l$ and $\zeta_0$ were set to be 0.01. The initial values of $\xi_0$ were set from $-0.5$ to $-11$, giving corresponding lines of the electric field. Some of the results are shown in Figure 1.